ISSN NO. 2320-5407

Journal homepage: http://www.journalijar.com

INTERNATIONAL JOURNAL OF ADVANCED RESEARCH

RESEARCH ARTICLE

Analytical Techniques For The Study Of Drug-DNA Interactions

Muhammad Sirajuddin[1], Ali Haider[2], *Saqib Ali[1]

1. Department of Chemistry, Quaid-i-Azam University, Islamabad 45320, Pakistan.

2. Department of Chemistry, Jacobs University, Bremen, Germany.

Manuscript Info

Manuscript History:

Received: 12 October 2013
Final Accepted: 26 October 2013
Published Online: November 2013

Key words:
Drug-DNA interaction; FT-IR spectroscopy; Viscometry; Thermal denaturation; Mass spectrometry; Atomic force microscopy

Corresponding Author

Saqib Ali

Abstract

Cancer chemotherapy was found on agents that interact with DNA or alkylate it, and such compounds continue to be clinically important today. The interactions between drugs and DNA have great importance in the study of their biological activity and have become an active research area in recent years. DNA is the material of bequest and control the structure and function of cells. Recently, there has been marvelous curiosity in studies related to the interaction of small molecules with nucleic acid because of their importance in the development of new reagents for biotechnology and medicine. The present study reviews a brief introduction to drug-DNA interactions, their types and various analytical techniques used to study the interaction between DNA and small ligand molecules that are potentially of pharmaceutical importance. Several instrumental techniques such as Infrared (IR), UV-Visible, Nuclear magnetic resonance (NMR) spectroscopies, Atomic force microscopy (AFM), Electrophoresis, Mass spectrometry, Viscosity measurements, UV Thermal denaturation studies, and Cyclic, Square wave etc., are used to study such interactions. Here we will discuss Infrared (IR), Mass spectrometry, Viscosity measurements, UV Thermal denaturation studies and Atomic force microscopy. The applications of spectroscopic techniques are reviewed and we have discussed the type of information (qualitative or quantitative) that can be obtained from the use of each technique. The information gained from this review might be useful for the development of potential survey for DNA structure and new therapeutic reagents for tumours and other diseases.

1. Structural features of DNA

Double-helical DNA consists of two complementary, anti-parallel, sugar–phosphate poly-deoxyribonucleotide strands which are associated with specific hydrogen bonding between nucleotide bases (Figure 1A). The two strands are held together primarily through Watson Crick hydrogen bonds where A forms two hydrogen bonds with T and C forms three hydrogen bonds with G (Figure 1B). The backbone of these paired strands defines the helical grooves, within which the edges of the heterocyclic bases are exposed. The biologically relevant B-form of the DNA double helix is characterized by a shallow–wide major groove and a deep–narrow minor groove. The chemical feature of the molecular surfaces in a given DNA sequence is distinct in either groove. This forms the basis for molecular recognition of duplex DNA by small molecules and proteins [1,2].

Figure 1: (A) Structure of DNA molecule. (B) Watson-Crick pairing between purine and pyrimidine bases in complementary DNA strands.

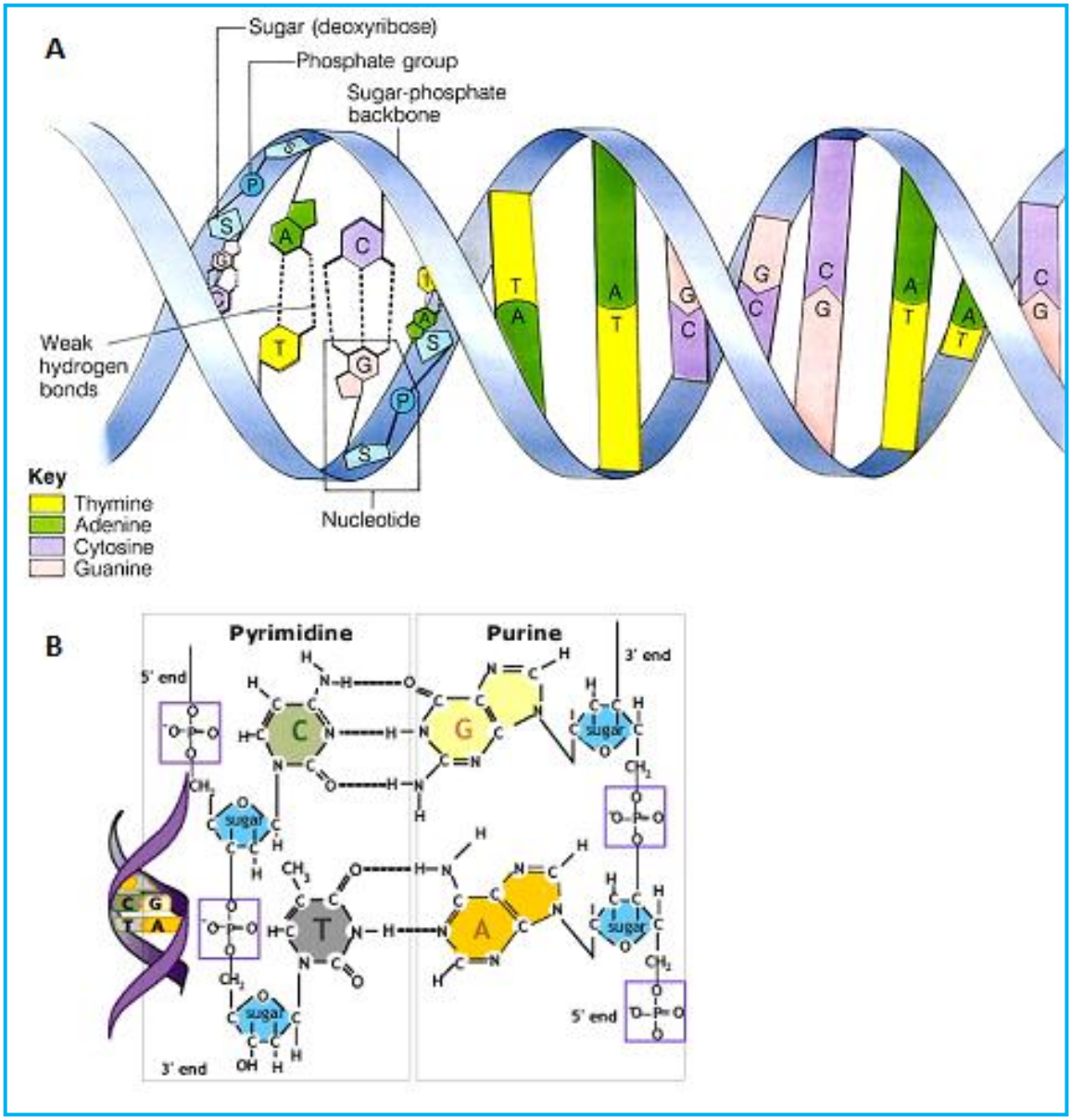

2. Drug-DNA Interactions and their types

Small ligand molecules bind to DNA and artificially alter and/or inhibit the functioning of DNA. These small ligand molecules act as drug when alteration or inhibition of DNA function is required to cure or control a disease [3]. Interaction study between drugs and DNA is very exciting and significant not only in understanding the mechanism of interaction, but also for the design of new drugs. However, mechanism of interactions between drug molecules and DNA is still relatively little known. It is necessary to introduce more simple methods for investigating the mechanism of interaction. By understanding the mechanism of interaction, designing of new DNA-targeted drugs and the screening of these in vitro will be possible [4]. Many of the most valuable anticancer drugs currently used in therapy interact with DNA either by a covalent or non-covalent mechanism. Unfortunately, several of them show a considerable toxicity when the DNA molecular target is present in both normal and tumor cells [5]. The covalent mode of binding of drug-DNA is irreversible and invariably causes the complete inhibition of DNA processes and subsequent cell death (if the reaction is not directly chemically reversible). A major advantage of covalent binders is the high binding strength. Moreover, covalent bulky adducts can cause DNA backbone distortion, which in turn can

affect both transcription and replication, such as by disrupting protein complex recruitment [6]. The covalent binders are also called alkylating agents due to adduct formation because they are used in cancer treatment to attach an alkyl group (C_nH_{2n+1}) to DNA [2]. Some important examples of covalent binder are given in Figure 2 [1].

Figure 2: Chemical structure of some covalent binder of DNA [1].

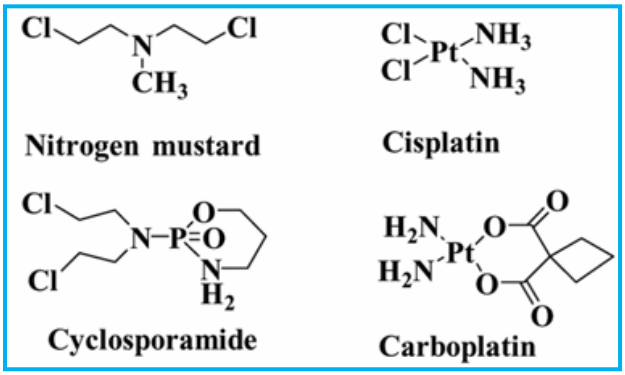

Figure 3: Chemical structure of some non-covalent binder of DNA [1].

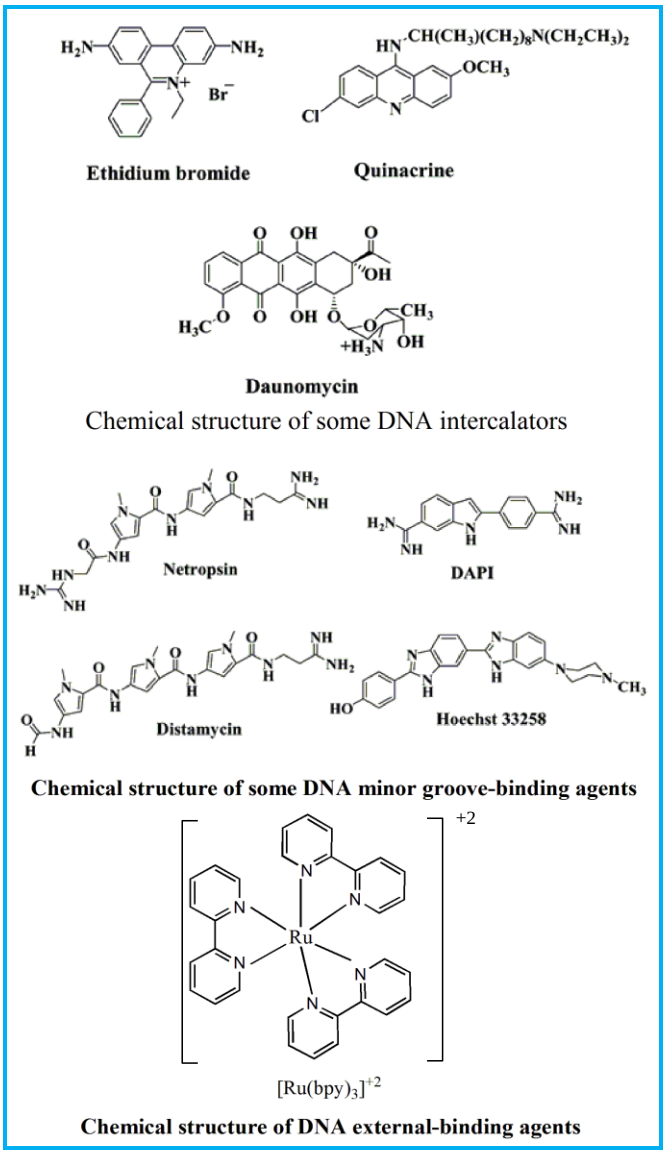

Non-covalent DNA interacting agents (groove binders, intercalators and external binders) are generally considered less cytotoxic than agents producing covalent DNA adducts and other DNA damage. The non-covalent binding mode is reversible and is typically preferred over covalent adduct formation keeping the drug metabolism and toxic side effects in mind. Non-covalent DNA interacting agents can change DNA conformation, change DNA torsional tension, interrupt protein–DNA interaction, and potentially lead to DNA strand breaks [7-9]. Some important examples of non-covalent binder are given in Figure 3 [1].

3. Techniques Used To Study Drug-DNA Interaction

This section consists of a list of the different instrumental techniques that have been used to study interactions between DNA and small ligand molecules. For each technique, we have provided a brief theoretical introduction to how it is applied to the study of the interactions, followed by a discussion of some examples that are characteristic of the technique or that are of specific interest.

Various techniques that are used to study the binding of drug molecules with DNA includes Infrared (IR), Raman, Circular dichroism, UV-Visible, Nuclear magnetic resonance (NMR) spectroscopies, Atomic force microscopy (AFM), Electrophoresis, Mass spectrometry, Viscosity measurements, UV Thermal denaturation studies, Cyclic, Square wave and Differential pulse voltammetry etc. These techniques have been used as a major tool to characterize the nature of drug-DNA complexation and the effects of such interaction on the structure of DNA. In the current review we will focus on: Infrared spectroscopy, UV Thermal denaturation, Viscometry, Atomic force microscopy and Mass spectrometry.

3.1. Infrared Spectroscopy

Fourier Transform Infrared (FT-IR) spectroscopy is a widely used technique to study interactions of nucleic acids (DNA and RNA) and proteins with anticancer drugs and other cytotoxic agents [10-15] in solutions. Infrared spectroscopy offers a variety of advantages. It can provide the details of molecular structures and intermolecular interactions with high resolution. It is not restricted by the size of the sample and can give valuable information for small biomolecules in complex biological systems. It can also generate structural information of the whole molecule in a single spectrum as a ‘‘photograph” of all conformations present in the sample. It can distinguish among A-, B-, and Z-forms of DNA, triple stranded helices, and other structural patterns. It is a powerful tool to study interactions of DNA with drugs and the effects of such interactions in the structure of DNA, providing some insights about the mechanism of drug action [16]. The technique is ideal for systematic studies of nucleic acids (e.g., sequence variations, covalent modifications), since it is fast, nondestructive, and requires only small amount of sample [17]. Infrared spectroscopy can be used to study biomolecules in different states, i.e., in solution, in solid and crystalline state or in monolayers making it possible to adapt the technique according to the specific requirement of the sample. Thus Infrared spectroscopy has the potential to investigate molecular events under conditions that are closely related to the physiological reaction environments.

The IR spectrum can be divided into four characteristic spectral ranges. The region from 1800 to 1550 cm^{-1} corresponds to the in-plane double bond vibrations of the nucleic bases (C=O, C=N, C=C and N-H bending vibrations of bases). These bands are sensitive to changes in the base stacking and base pairing interactions. Bands occurring in the interval 1500-1250 cm^{-1} assigned to vibrations of the bases and base-sugar connections are strongly related to the conformational changes of the backbone chain and glycosidic bond rotation. The range 1250-1000 cm^{-1} involves sugar phosphate vibrations, such as PO_2 symmetric and asymmetric stretching vibrations and C-O stretching vibrations. These vibrations show high sensitivity to conformational changes in the backbone. The range 1000-800 cm^{-1} is characteristic for bands associated with vibrations of sugars which correlate with the various nucleic acid sugar puckering modes (C2'-endo and C3'-endo) [18-24].

The region of interest in IR studies dealing with DNA in aqueous solutions is between 1800 and 800 cm^{-1}. Due to interfering absorption bands of water at 1650 cm^{-1} and below 950 cm^{-1}, spectra are generally recorded also in D_2O, where these bands move to 1200 cm^{-1}, and below 750 cm^{-1}. Combination of results from both spectra allows obtaining a complete spectrum. The use of D_2O also causes shifts in nucleic acid absorptions, resulting from deuterium exchange of labile NH protons, and these can be used to monitor H-D exchange processes. A method to remove water signals in the spectra is water substraction, using a NaCl solution as reference. The characteristic IR bands of nucleic acids have been compiled and discussed in Table 1 [25]; four regions are considered, each one containing marker bands reflecting either nucleic acid interactions and/or conformations, as shown in Figure 4.

Figure 4: Approximate position of IR bands of DNA and aqueous solvents. a) 1800-1500 cm^{-1} region, sensitive to effects of base pairing and base stacking. b) 1500-1250 cm^{-1} region, sensitive to glycosidic bond rotation, backbone conformation and sugar pucker. c) 1250-1000 cm^{-1} region, sensitive to backbone conformation. d) 1000-800 cm^{-1} region, sensitive to sugar conformation [25].

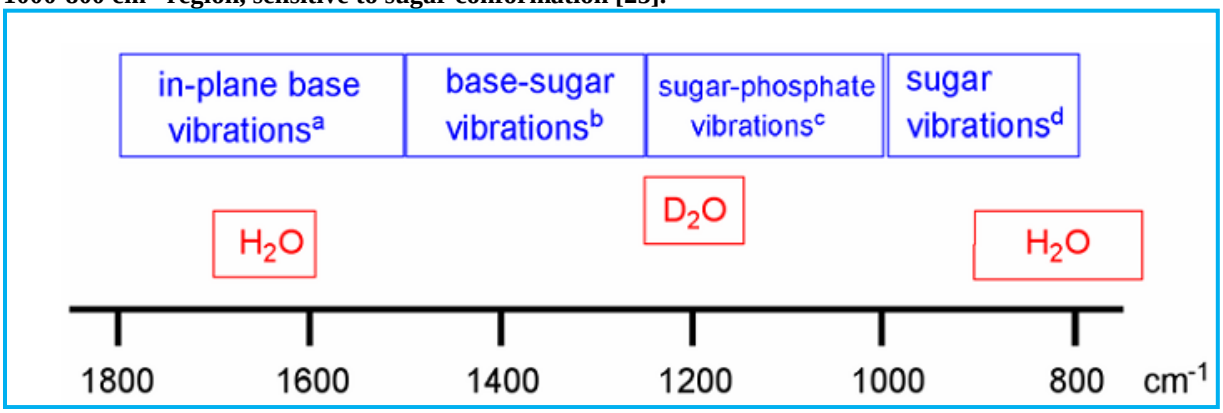

Table 1: The wavenumbers and spectral assignments of selected IR bands in nucleic acids. The comment column gives the basis for the assignment. Typical relative intensities are given in parentheses for certain bands[a] [25]

Wavenumber (cm^{-1})	Assignment	The 1800–1500 cm^{-1} region in DO_2 In-plane base vibrations Sensitive to effects of base pairing and base stacking Comment
1715	G*G–C/ts	C6=O6 str of G involved in Hoogsteen third strand binding
1712	T*A–T/ts	C2=O2 str of T involved in reverse Hoogsteen third strand binding
1710	C^+*G–C/tc	C2=O2 str of protonated C involved in Hoogsteen third strand binding
1698–1691	U, T/ss	C2=O2 str of U/ss or ds (medium)
	U, T/ds	C2=O2 str of T/ss or ds (medium) Calc: C2=O2 str of U
1689–1678	G/ds	C=O6 str of G/ds (medium)
1677–1672	U/ds	C4=O4 str U/ds (medium)
1673–1660	G/ss	C6=O6 str of G/ss (strong)
1671–1655	T/ss	C4=O4 str of T/ss (strong) or T/ds (medium) C4=O4 str of U/ss (strong)
1657–1653	U/ss	Shifts to 1672 and decrease in intensity upon duplexation Calc: C4=O4 str of U, coupled with C4–C5 str
1655–1647	C/ss	C2=O2 str of C/ss (strong) or ds (medium)
	C/ds	Small downshift (1652 to 1649) and decrease in intensity upon duplexation
1645–1641	T/ds	In-plane ring vib of T/ds
1632	T/ss	In-plane ring vib of T/ss
1632–1622	A/ss	C=N; C=C ring vib of A/ss (strong) and ds (medium) Decrease in intensity upon duplexation
	A/ds	Shifts 1626 to 1622 upon duplexation in DNA and 1628 to 1631 upon duplexation in RNA Calc: C4=C5, C5–C6 out-of-phase ring vib of A
1624–1616	C/ss	In-plane ring vib of C/ss (medium) or ds (weak)
	C/ds	Calc: C4–C5, C5_C6 out-of-phase ring vib of C
1618–1615	U/ss	In-plane ring C=C str of U/ss (weak) Calc: suspected combination band (1258+364/352) of U
1590–1575	G/ss	C=N ring vib of G/ss (strong) and ds (weak)
	G/ds	Decrease in intensity upon duplexation

		Calc: C4=C5, C5–C6 in-phase ring vib of G
1585–1582	C	In-plane ring vib of C (weak)
1579–1576	A	In-plane ring vib of A (weak)
		Calc: C4=C5, C5–C6 in-phase ring vib of A
		C=N ring vib of G/ss (medium) and ds (weak)
1568–1564	G/ss	Decrease in intensity upon duplexation
	G/ds	Calc: C6=O6, C5–C6 in-phase str coupled with C4=C5 out-of phase str of G
		In-plane vib of C/ss (medium) and ds (weak)
1527–1520	C/ss	Drastic decrease in intensity upon duplexation
	C/ds	Calc: skeletal out-of-phase vib of C

a) Abbreviations: G: guanine; A: adenine; C: cytosine; U: uracil; ts: triple-stranded; ds: double-stranded; ss: single-stranded; calc: calculation; str: stretch; vib: vibration; def: deformation; symm: symmetric; asymm: asymmetric; d: deoxyribose; r: ribose.

Spectral features of carboplatin–DNA complexes are shown in Figure 5 [26]. Ring vibrations of nitrogenous bases (C=O, C=N stretching), PO_2 stretching vibrations (symmetric and asymmetric) and deoxyribose stretching of DNA backbone are confined in the spectral region 1800–700 cm^{-1}. The vibrational bands of DNA at 1710, 1662, 1613 and 1492 cm^{-1} are assigned to guanine (G), thymine (T), adenine (A) and cytosine (C) nitrogenous bases, respectively [27-31]. Bands at 1228 and 1087 cm^{-1} denote phosphate asymmetric and symmetric vibrations, respectively. These are the prominent bands of pure DNA, which are monitored during carboplatin–DNA interaction at different ratios in this study. Changes in these bands (shifting and intensity) are shown in Fig. 5. After carboplatin addition to DNA solution, guanine band at 1710 shifts to 1702–3, thymine band at 1662 shifts to 1655 and adenine band at 1613 shifts towards lower wave number 1609–10 cm^{-1}. These shifting can be attributed to direct platin binding to guanine (N7), thymine (O2) and adenine (N7) of DNA bases. No major shifting is observed for phosphate asymmetric and symmetric vibrations indicating no external binding. The plots of the relative intensity (R) of several peaks of DNA in-plane vibrations related to A-T, G-C base pairs and the PO_2^- stretching vibrations such as 1717 (guanine), 1663 (thymine), 1609 (adenine), 1492 (cytosine), and 1222 cm^{-1} (PO_2^- groups), *vs.* the compound concentrations can be obtained after peak normalization using the equation:

$$Ri = \frac{Ii}{I968}$$

where Ii is the intensity of absorption peak for pure DNA and DNA in the complex with i concentration of compound, and I_{968} is the intensity of the 968 cm^{-1} peak (internal reference) [30].

Figure 5: (A) Stacked view of FT-IR spectra of free calf-thymus DNA and carboplatin/DNA ratios of 1/100, 1/50 and 1/10 in the region of 1800–700 cm^{-1}. (B) Intensity ratio variations for DNA as a function of different carboplatin/DNA molar ratios [26].

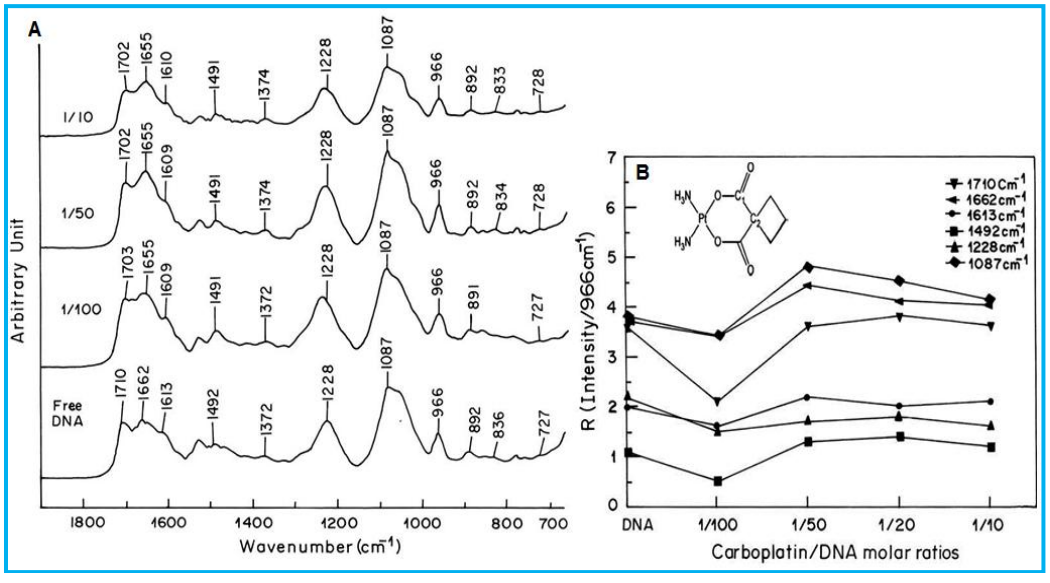

Similarly the FT-IR spectra of methylene blue-DNA, acridine orange-DNA and ethidium bromide-DNA are given in Figure 6a-c [31].

Evidence for methylene blue (MB) and ethidium bromide (EB) intercalation into DNA base pairs comes from minor intensity increase of DNA in-plane vibrations at 1717 (G), 1663 (T), 1609 (A), and 1222 cm^{-1} (PO_2 asymmetric stretch) upon pigment interaction (Figures 6a and 6c). While that for the intercalation of acridine orange into DNA base pairs comes from minor intensity increase of DNA vibrations at 1717 (G) and 1222 cm^{-1} (PO_2 stretch) upon dye complexation (Figure 6b). The major shifting of the guanine band at 1717 to 1713 cm^{-1} for MB, at 1717 to 1712 cm^{-1} for AO and at 1717 to 1710 cm^{-1} for EB, respectively is an indication of dye intercalation mainly into the GC base pairs (Figures 6a-c(A). The thymine band at 1663 cm^{-1} exhibited no shifting upon dye complexation in case of MB and AO. The adenine band at 1609 cm^{-1} was overlapped with strong pigment absorption band at 1600 cm^{-1} both in MB and AO, which makes it difficult to draw a certain conclusion on the nature of dye interaction with A–T bases. In case of EB shifting is observed in thymine band at 1663 to 1662 cm^{-1} and adenine band at 1609 to 1605 cm^{-1}, respectively which are due the intercalation of EB into AT base pair in addition to GC base pair. The shifting of the PO_2 asymmetric band at 1222 to 1224 cm^{-1} for MB, 1222 to 1227 cm^{-1} for EB respectively with some increase in intensity of this vibration is due to their interaction with the backbone PO_2 groups (external binding). The overall binding constants (K) calculated for MB, AO and EB are: K(MB–DNA) = 2.13 x 10^4 M^{-1}, K(AO–DNA) = 2.69 x 10^4 M^{-1}, and K(EB–DNA) = 6.58 x 10^4 M^{-1}, respectively. The larger K value for EB–DNA is due to greater accessibility of ethidium bromide for DNA binding rather than MB and AO [31].

Figure 6a: (A) FTIR spectra and different spectra of calf-thymus DNA and its complexes with methylene blue (MB) in the region of 1800–600 cm^{-1} at different pigment/DNA (P) molar ratios and (B) the intensity ratio variations for several DNA vibrations 1717 (G), 1663 (T), 1609 (A), 1492 (C and G) and 1222 cm^{-1} (PO_2 stretch) as a function of pigment concentrations [31].

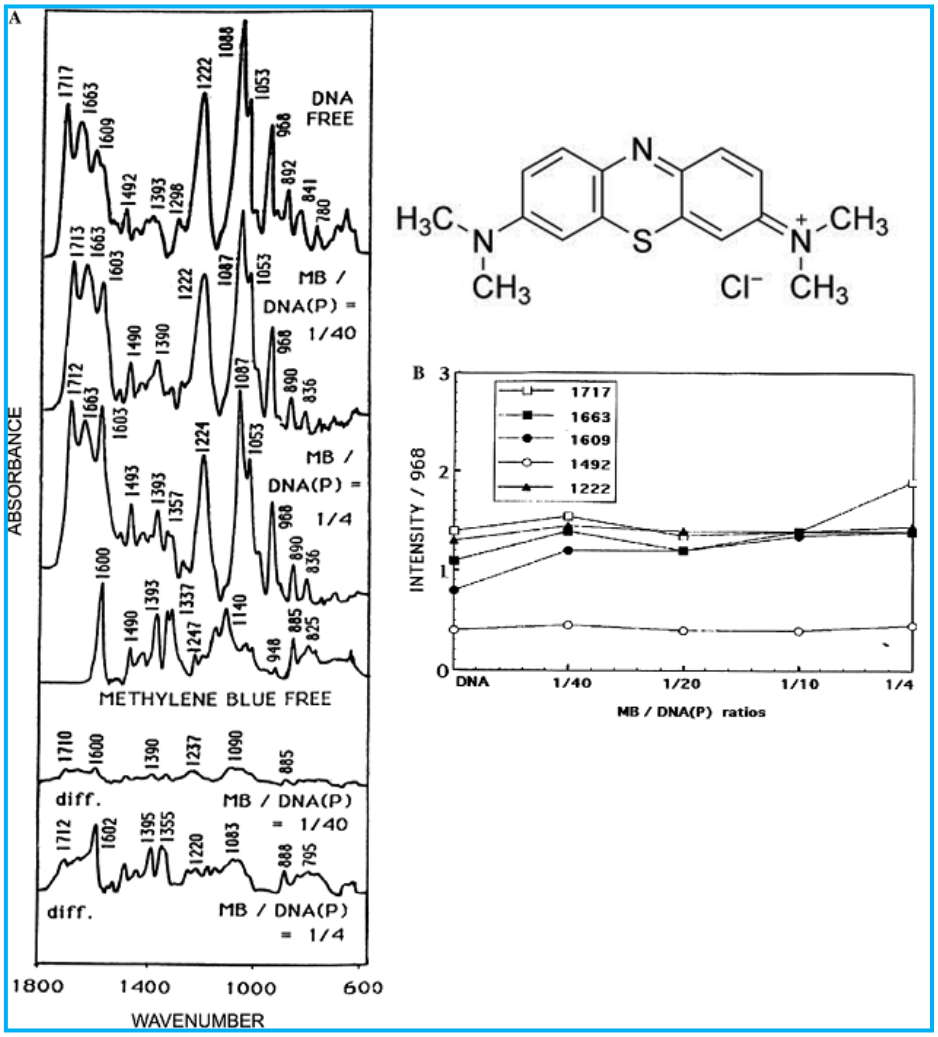

Figure 6b: (A) FTIR spectra and different spectra of calf-thymus DNA and its complexes with acridine orange (AO) in the region of 1800–600 cm^{-1} at different pigment/DNA (P) molar ratios and (B) the intensity ratio variations for several DNA vibrations 1717 (G), 1663 (T), 1609 (A), 1492 (C and G) and 1222 cm^{-1} (PO_2 stretch) as a function of pigment concentrations [31].

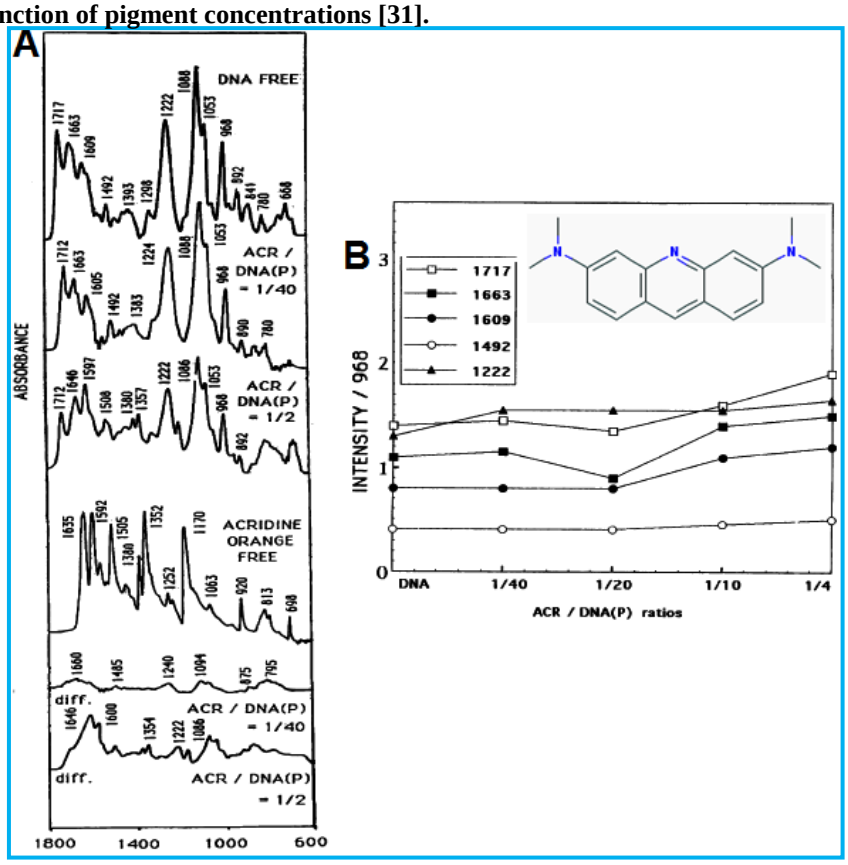

Figure 6c: (A) FTIR spectra and different spectra of calf-thymus DNA and its complexes with ethidium bromide (EB) in the region of 1800–600 cm^{-1} at different pigment/DNA (P) molar ratios and (B) the intensity ratio variations for several DNA vibrations 1717 (G), 1663 (T), 1609 (A), 1492 (C and G) and 1222 cm^{-1} (PO_2 stretch) as a function of pigment concentrations [31].

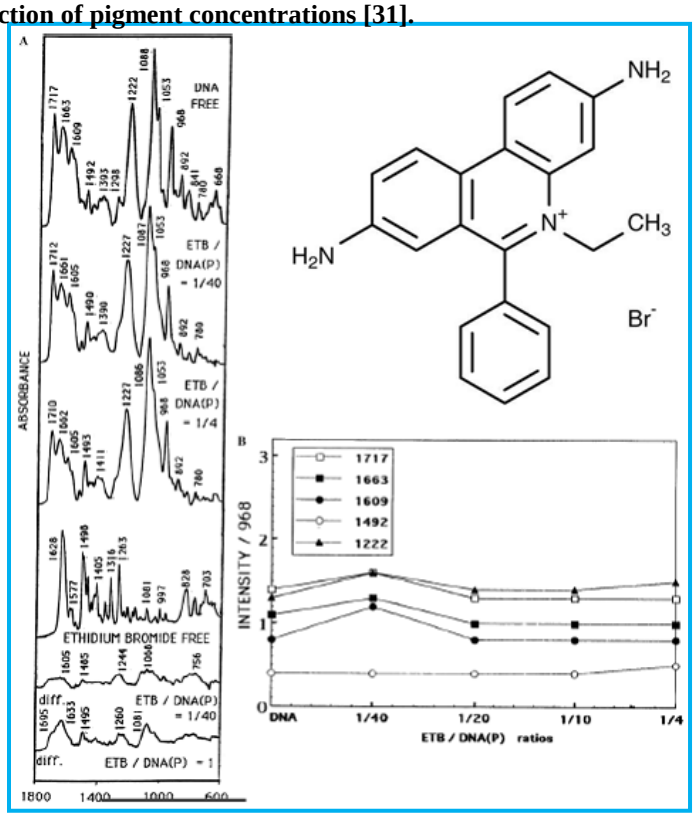

Figure 7 represents the interaction of zanamivir (also known as neuroaminidase NA) DNA. At low zanamivir concentration (r = 1/20), minor drug–DNA interaction occurs. Confirmation for this comes from the spectral changes (intensity or shifting) of several polynucleotides in-plane vibrations related to the G-C, A-T bases and the backbone phosphate modes at 1710 (mainly G), 1662 (mainly T), 1610 (A), 1492 (mainly C), and 1226 (asymmetric PO_2 vibration) and 1088 cm^{-1} (PO_2 symmetric vibration) in the presence of zanamivir. At r = 1/20, shifting for the bands at 1710 (guanine) to 1706, 1662 (thymine) to 1658, 1610 (adenine) to 1607, 1492 (cytosine) to 1493, and 1226 (asymmetric stretching phosphate) to 1229 cm^{-1} were observed (Figure 7A). The observed shiftings were accompanied by a decrease in intensities of guanine band (7%), thymine band (5%), adenine band (8%), cytosine band (14%), PO_2 (asym) (7%), and PO_2 (sym) (5%) (Figure 7B). A minor loss of intensity of the DNA in plane vibrations can be attributed to partial helix stabilization as a result of drug–DNA complexation.

As zanamivir concentration increased (r = 1/10), shiftings for the bands at 1710 (guanine) to 1703, 1662 (thymine) to 1656, 1610 (adenine) to 1606, 1492 (cytosine) to 1494, 1226 (PO_2 asymmetric) to 1229, and 1088 (PO_2 symmetric) to 1087 cm^{-1} were observed in the spectra of zanamivir–DNA complexes. Some increases in the intensities of adenine, guanine, cytosine and thymine bands were observed. The spectral changes can be related to zanamivir interaction with GC and AT base pairs. The phosphate bands at 1226 (asym PO_2), 1088 cm^{-1} (sym PO_2) showed no major intensity changes upon drug interaction. The increase in the intensities of the bands at 1710 (G), 1662 (T), 1610 (A), and 1492 cm^{-1} (C), continued up to r = 1/5, indicating major zanamivir interaction with guanine, thymine, adenine, and cytosine. No major intensity changes were observed for the PO_2 symmetric and asymmetric bands (Figure 7A). At high drug concentration, r = 1/2, some reduction in the intensity ratios of the bands at 1710 (G), 1662 (T), 1610 (A), and 1492 cm^{-1} (C) were observed. The observed loss of intensity ratios were probably due to helix stabilization induced by the interaction of zanamivir with the DNA, no major intensity change was observed for phosphate group. A similar increase in the intensity ratios of several DNA vibrations was also observed when DNA was incubated with high concentrations of chlorophyll and diethtylstlbestrol [4,4'-(3*E*)-hex-3-ene-3,4-diyldiphenol]. As concentration increased (r = 1/1), major increase in the intensities of adenine and thymine was observed which is indicative of major interaction with A-T base pairs (minor groove). Minor increase in the intensities of guanine and cytosine, asymmetric and symmetric phosphate are indicative of some degree of drug interactions with G-C bases and phosphate group [32].

Figure 7: (A) FTIR spectra in the region of 1800–600 cm^{-1} for free calf thymus DNA, zanamivir, and zanamivir adducts in aqueous solution at pH 6.5–7.5 (top four spectra) and difference spectra obtained at various zanamivir–DNA phosphate) molar ratios (bottom two spectra); (B) Intensity ratio variations for several DNA in-plane vibrations as a function of zanamivir concentration. Intensity ratios for the DNA bands at 1710 (G,T), 1662 (T,G, A,C), 1610 (A), 1492 (C,G), 1226 (PO_2 asymmetric stretch), and 1088 cm^{-1} (PO_2 symmetric stretch) referenced to the DNA band at 968 cm^{-1} [32].

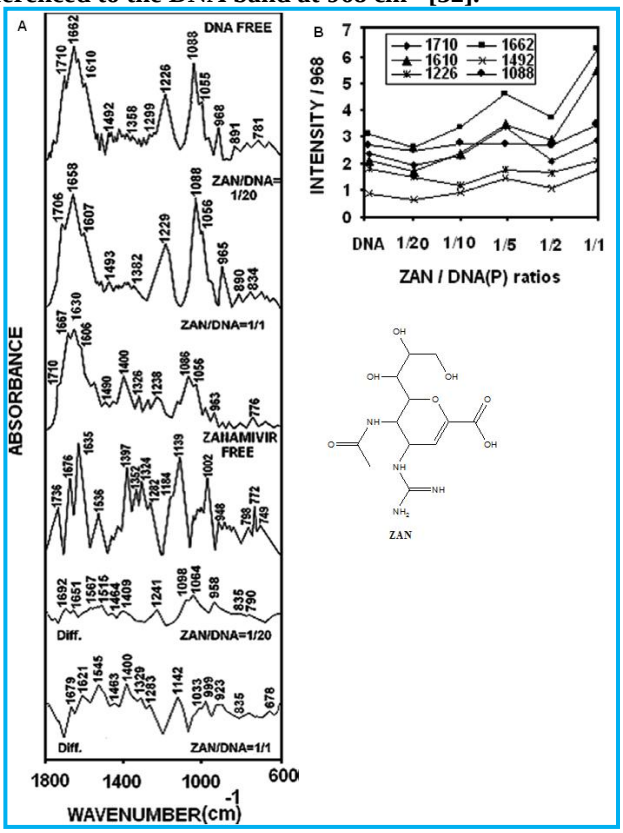

3.2. Viscosity Measurements

DNA viscosity is sensitive to DNA length change; therefore, its measurement upon the addition of a compound is often concerned as the least ambiguous and most critical method to clarify the interaction mode of a compound with DNA and provides reliable evidence for the intercalative binding mode. Relative viscosity measurements have proved to be a reliable method for the assignment of the mode of binding compounds to DNA. In the case of classical intercalation, DNA base pairs are separated in order to host the bound compound resulting in the lengthening of the DNA helix and subsequently increased DNA viscosity, i.e., a classical intercalation model requires the space of adjacent base pairs to be large enough to accommodate the bound ligand and elongate the double helix, resulting in an increase of DNA viscosity [33,34]. On the other hand, the binding of a compound exclusively in DNA grooves by means of partial and/or non-classic intercalation, under same conditions, (e.g., netropsin, distamycin), causes a bend or kink in the DNA helix and reducing its effective length and, as a result, DNA solution viscosity is decreased or remains unchanged, i.e., groove binders do not lengthen the DNA molecules [35-39].

Figure 8 shows the interaction of Three Schiff base compounds of *N*'-substituted benzohydrazide and sulfonohydrazide derivatives: *N*'-(2-hydroxy-3-methoxybenzylidene)-4-*tert*-butylbenzohydrazide (1), *N*'-(5-bromo-2-hydroxybenzylidene)-4-*tert*-butylbenzohydrazide (2) and N'-(2-hydroxy-3-methoxybenzylide-ne)-4-methylbenzenesulfonohydrazide (3) with SS-DNA. This may be explained by the insertion of the compounds in between the DNA base pairs, leading to an increase in the separation of base pairs at intercalation sites and, thus, an increase in overall DNA length [40-42].

Figure 8: (A) Effects of increasing amount of Compounds (1-3) on relative viscosity of SSDNA at 25 ± 0.1 °C. [DNA] = 7.2 µM, r = 0, 6.9, 13.9, 20.8, 27.8 [40].

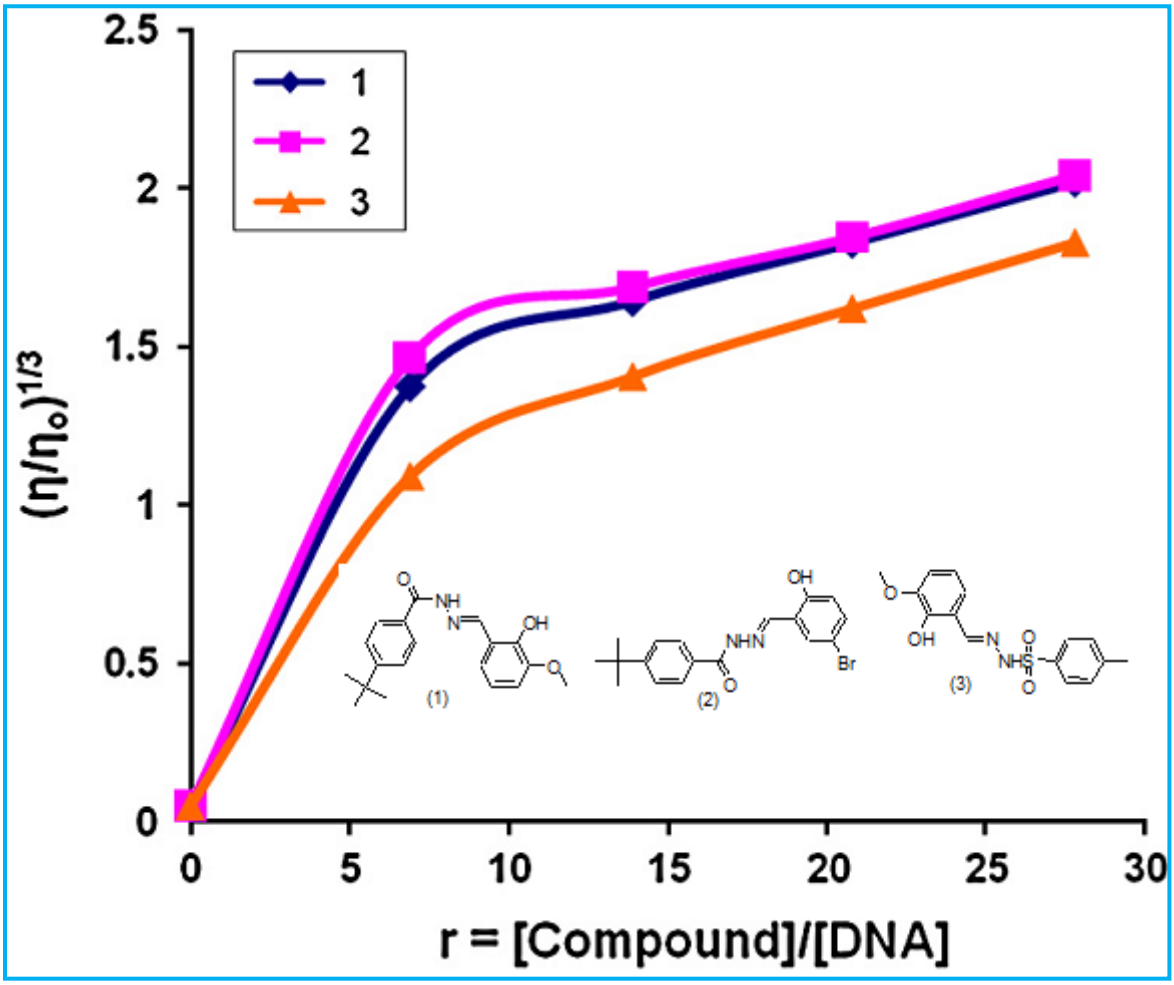

Figure 9A shows the plot of relative specific viscosity $(\eta/\eta_o)^{1/3}$ versus 1/R (R = [DNA]/[complex]), in the absence and in the presence of Ni(II) complex. The viscosity data show that there are at least two phases of binding between the complex and CT-DNA. At lower concentration of the complex, the viscosity first decreases and then increases at higher concentration of complex. This slow increase in viscosity is an indication of groove binding [43].

In Figure 9B it is shown that with increasing amount of 3-((3,5-dimethylphenylimino)methyl)benzene-1,2-diol (HL), the relative viscosity of DNA first remains constant and then increases which supports that HL bind through intercalation mode but with different affinity, i.e., also show some affinity for binding with grooves of DNA through hydrogen bonding, typically to N3 of adenine and O2 of thymine. However, strong binding is presumably due to intercalation with DNA [44].

Figure 9: (A) Effect of increasing amounts of Ni(II) complex on the viscosity of CT-DNA (5 x 10^{-5} M) in 10 mM Tris buffer [43]. (B) Effects of increasing amount of HL on relative viscosity of CT-DNA at 25 ± 0.1°C. [DNA] = 2.37×10^{-5} M [44].

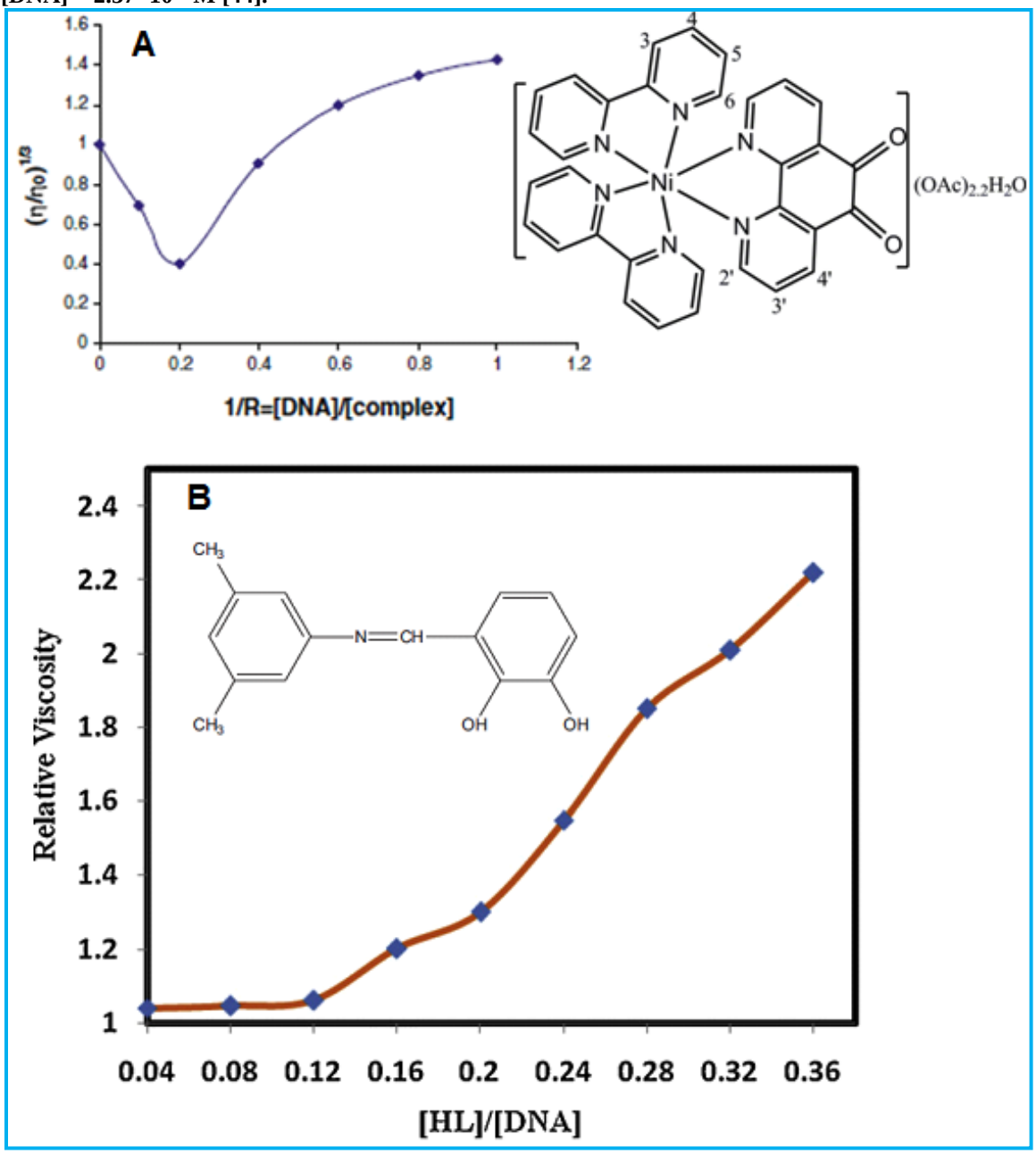

Figures 10 and 11 show the electrostatic binding mode of nickel and organotin(IV) complexes with DNA, respectively. The viscosity of DNA remains essentially unchanged on the addition of the nickel complexes while it decreases in case of organotin(IV) complexes [45,46].

Figure 10: Effect of increasing amount of the complexes [Ni(hhmh)$_2$] (1), [Ni (bhmh)$_2$] (2), [Ni(ihmh)$_2$] (3), [Ni(PPh$_3$)(hpeh)] (4), [Ni(PPh$_3$)(bpeh)] (5), [Ni(PPh$_3$)(ipeh)] (6) on the relative viscosity of HS-DNA at 16(±0.l) ^{o}C [45].

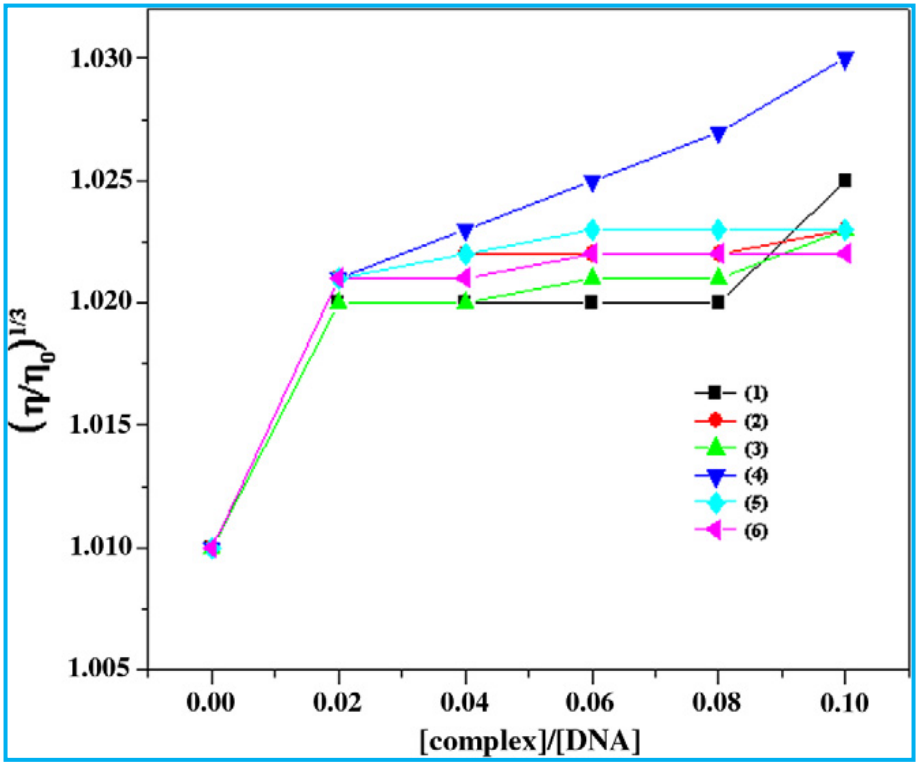

Figure 11: Effects of increasing amount of Tri-*n*-buthyltin(IV) 3-[(3',5'-dimethylphenylamido)]propanoate (compound 2) and Triphenyltin(IV) 3-[(3',5'-dimethylphenylamido)]propanoate (compound 3) on relative viscosity of SS-DNA at 25 ± 0.1 ^{o}C. [DNA] = 1.86×10^{-4}M [46].

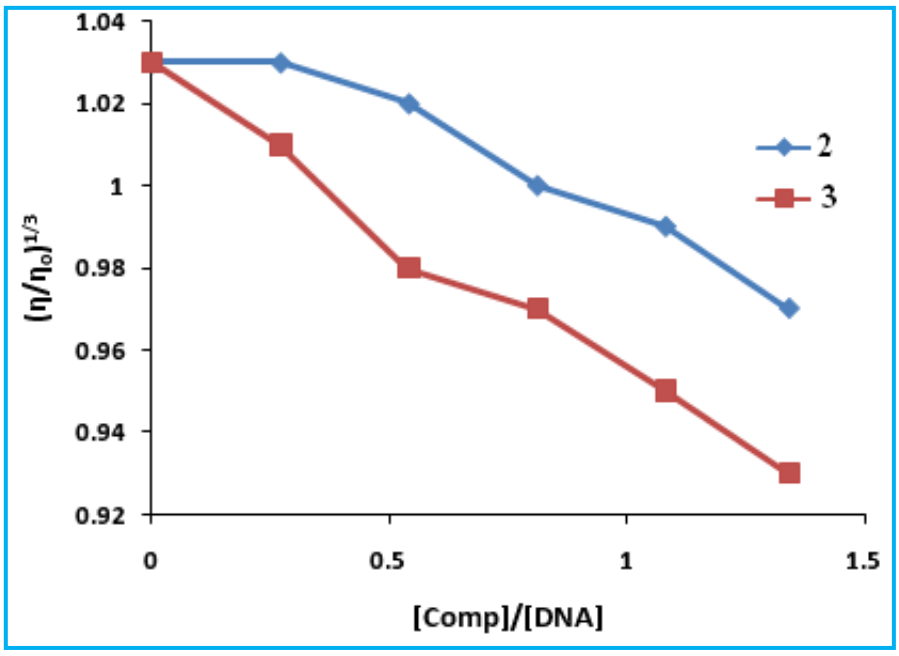

3.3. UV Thermal denaturation studies

The melting temperature, *Tm*, which is defined as the temperature at which the double helix denatures into single-strand DNA or the temperature where half of the total base pairs are unbonded. The extinction coefficient of DNA bases at 260 nm in the double-helical form is much less than that in the single strand form, hence, melting of the helix leads to an increase in the absorption at this wavelength. Thus, the melting temperature can be determined by monitoring the absorbance of the DNA bases at 260 nm as function of temperature. Intercalation of small molecules into the double helix is known to increase the helix melting temperature [47]. When the temperature in solution increases, the double-stranded DNA gradually dissociates to single strands, and results in hyperchromic effect on the absorption spectra of DNA base pairs ($\lambda = 260$ nm). A large change in the *Tm* of DNA indicates a strong interaction between the complexes and DNA. DNA melting experiments are useful in establishing the extent of intercalation. Intercalation of the complexes into DNA causes stabilization of base stacking and hence raises the melting temperature of the double-strand DNA [48].

Figure 12A shows the thermal denaturation profiles of CT-DNA in the absence and presence of complexes mer-[$RuCl_3$(dmso)(bpy)] (1), mer-[$RuCl_3$(dmso)(phen)] (2), and mer-[$RuCl_3$(dmso)(dppz)] (4) with the profile of mer-[$RuCl_3$(dmso)(dpq)] (3) included for comparison purpose (salt concentration: 0.01 M $NaClO_4$). In the absence of Ru(III) complexes, CT-DNA shows a main transition at *Tm* = 68.1 °C. No distinct increase in the melting temperature is observed in the presence of 1 and 2, while the *Tm* of CT-DNA is increased upon addition of 4. The increase is more pronounced for the addition of 4 (ΔTm = 10.8 °C) than that of 3 (ΔTm = 5.3 °C). The large increased ΔTm suggest an intercalative binding of 4 to DNA. *Tm* depends on the salt concentration [49]. Compound 4 under different ionic strength shows different *Tm*. In salt concentrations of 0.1 M $NaClO_4$ it shows less profound increase in *Tm* (ΔTm = 7.5 °C) while at higher salt concentrations (0.2 M $NaClO_4$) there is no change in *Tm*. Three factors may account for the thermal stability of DNA modified by metal complexes, including: stabilizing effects of the positive charge on the metal moiety and of DNA interstrand cross-links, a destabilizing effect of conformational distortions such as intrastrand cross-links by platinum coordination, and the presence of potential intercalative ligands should also be taken into account in this case. The electrostatic effects of the Ru(III) complexes are lowered with increasing concentration of Na^+ counter ions, and the relatively unchanged *Tm* is a consequence of competition between the stabilizing effects and the destabilizing effects [47,50].

The interactions of ruthenium(II) complexes with CT-DNA are characterized by measuring the effects on melting temperature of DNA (Figure 12B). In the absence of any added complexes, the thermal denaturation determined for DNA gave a *Tm* of 61.30 ± 0.54 °C. The observed melting temperatures in the presence of complexes [$Ru(dmb)_2$(DBHIP)](ClO_4)$_2$ (1) and [$Ru(dmp)_2$(DBHIP)](ClO_4)$_2$ (2) were 67.30 ± 0.50 and 66.99 ± 0.53 °C, respectively. The increase in *Tm* of the two Ru(II) complexes (the ΔTm is 6.00 and 5.69 °C for 1 and 2) provides a strong support for intercalation into the helix of DNA [51].

Figure 12: (A) Thermal denaturization curves of CT-DNA (60.0 µM) at the concentration ratios of [Ru]/[DNA] = 1/10. (■ for DNA alone; ⬭ for 1 and DNA; □ for 2 and DNA; ▲ for 3 and DNA ; ♦ for 4 and DNA) [47]. (B) Thermal denaturation of CT-DNA in the absence (filled square) and presence of complexes 1 (filled circle) and 2 (filled triangle). [Ru] = 32 µM, [DNA] = 80 µM [51].

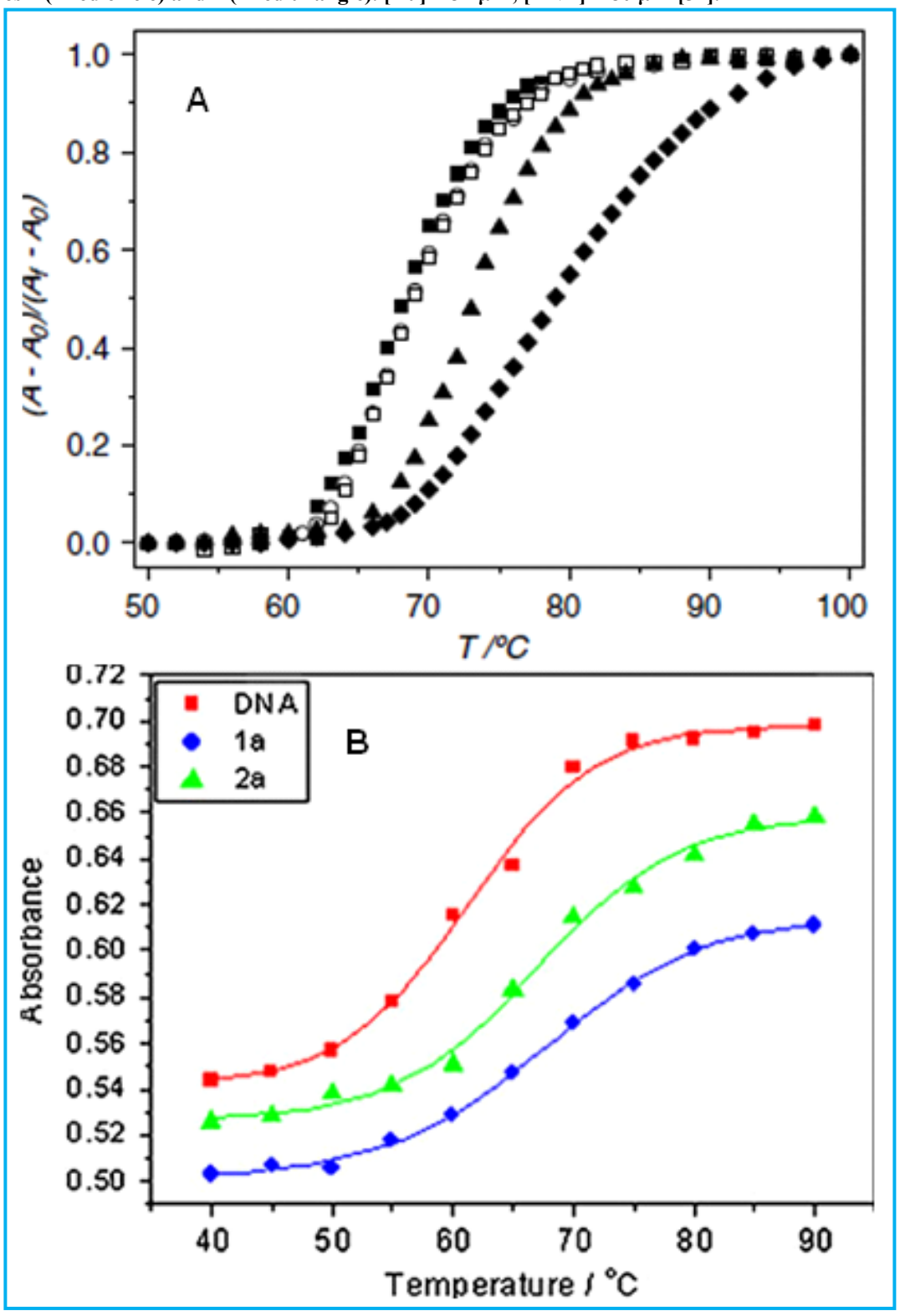

3.4. Mass Spectrometry

Mass spectrometry (MS) has become one of the most common techniques adopted to study interactions between DNA and small ligand molecules. The ability of mass spectrometry to investigate drug-DNA interactions have been reviewed recently [52,53]. The binding stoichiometry, the relative binding affinities and the binding constants for DNA double helices of various sequences may be determined [54,55]. Electrospray ionization (ESI) is the most common ionization method used in the study of biomolecules due to its soft ionization [56-58]. Using ESI techniques, biomolecules can be transferred from the solution to the mass spectrometer with minimal fragmentation and, so, both the mass of the DNA and the mass of the DNA-ligand complex can be determined as the non-covalent interactions that formed the complex are not altered during the electrospray process [59]. Focusing on the use of ESI-MS to study complexes, MS gives a signal for each species with a different mass and so it is very straightforward to establish the stoichiometry of the complexes. ESI-MS signals enable several calculations to be performed: the number of DNA strands involved, the number of bound cations (if present) and the number of bound ligands, among others.

Taking into account the structure of the nucleic acids, ESI-MS studies are performed using negative polarity. It is well known that the phosphodiester backbone of DNA has a pKa value below 1 and it is fully deprotonated under usual working conditions. In general, in order to preserve their structure, nucleic acid solutions are prepared with monovalent ions. As ESI presents a low salt tolerance, the use of ammonium acetate is preferred because of its good compatibility with ESI-MS.

Figure 13 shows the structures of various anticancer drugs that are structurally specific for the G-quadruplex or duplex DNA recognition. Perylene derivatives, such as *N,N-bis*-(2-(dimethylamino)ethyl)-3,4,9,10-perylenetetracarboxylic acid diimide (DAPER, P1), favor π–π interactions with the G-tetrad surface. 5,10,15,20-*tetrakis*-(1-methyl-4-pyridyl)-21H,23H-porphine (TMPyP4, P5) is an effective telomerase inhibitor (having EC50 value of 6.5 mm in a cell-free assay) also binds to the G-quadruplex in the c-myc promoter. Polyamides (such as ImImImbDp (P6)) derived from distamycin A have been extensively explored for recognition and binding with high affinity in the minor groove of predetermined duplex-DNA sequences [60-65].

Figure 14 shows the ESI mass spectrum of the G-rich sequence (S1) in a 20 mm ammonium acetate solution shows a dominant peak for the G-quadruplex ion with two NH_4^+ ions, $[S1+2NH_4^+-7H^+]^{5-}$. Since cations are known to sit between two G-tetrad layers and to stabilize the G-quadruplex structure, it would be reasonable to assume that there are three tetrad layers in a G-quadruplex possessing two NH_4^+ ions [66]. Similarly Figure 15 shows parts of the mass spectra of the G-quadruplex DNA with two small molecules in a molar ratio of 1:4 as examples. For the cationic porphyrin P5, the intense signal of the 1:2 complex ion ($[G+2P5]^{5-}$ at m/z 1737) is the base peak (Figure 15A), and the free G-quadruplex ion is not observed in the spectrum. For P7, the signal of the 1:1 complex ion at m/z 1547 is the base peak, whereas the free G-quadruplex and its 1:2 complex ion have intensities of 82% and 38%, respectively (Figure 15B). Therefore, the ESI-MS results show that P5 has notable specificity with a 1:2 binding stoichiometry when the concentration of the small molecule reaches 40.0 mm [60].

Figure 13: Structures of the seven small molecules studied (P1–P7) [60].

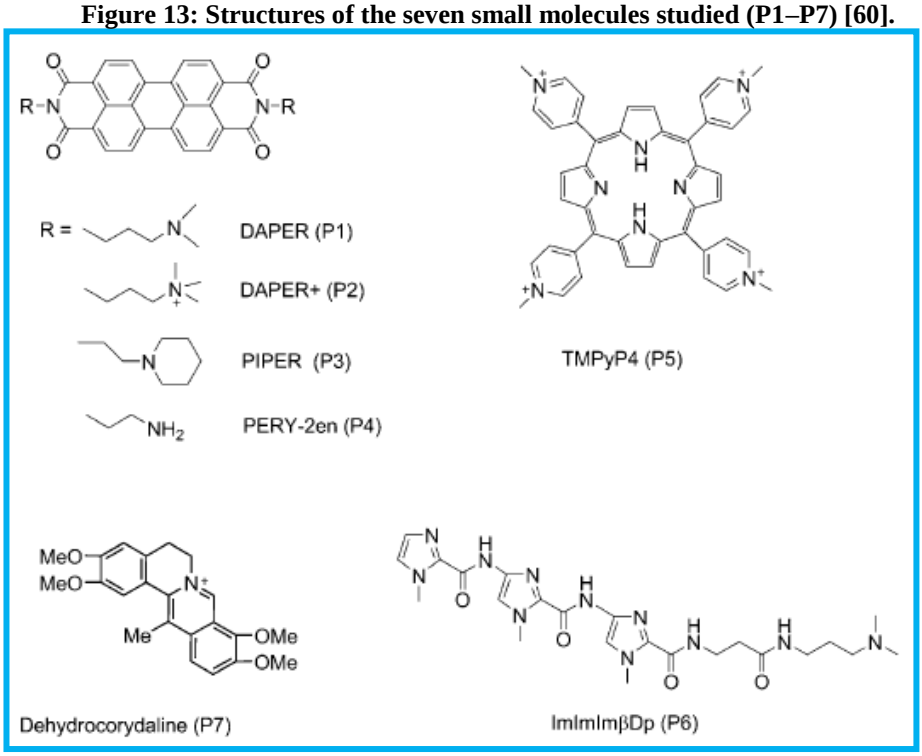

Figure 14: ESI mass spectrum of the G-rich sequence (S1) in 20 mm NH_4OAc buffer (pH 7.0), S1 = dGGGCGCGGGAGGAAGGGGGCGGG [60].

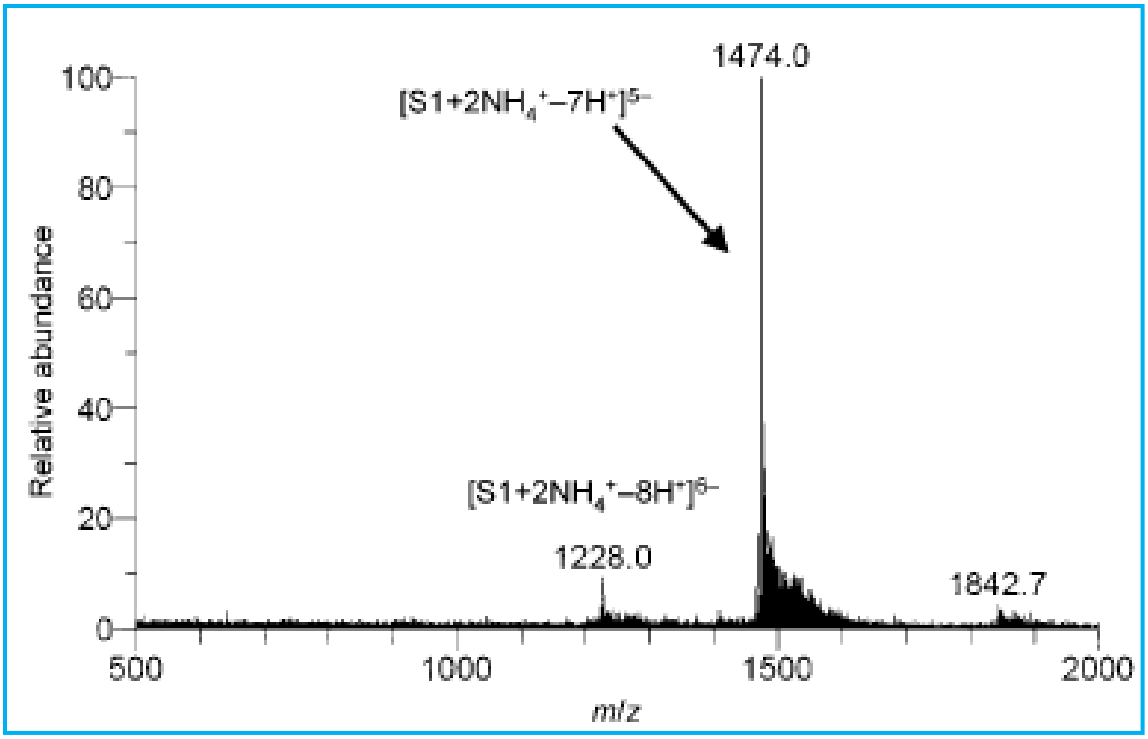

Figure 15: ESI mass spectra of 10.0 mm S1 DNA with a 40.0 mm concentration of small molecules A) P5 and B) P7. [G]: G-quadruplex ion; [G+*n*Pi]: a 1: *n* complex ion of the G-quadruplex (G) and the small molecule Pi (*n* =1 or 2).
G-rich sequence, S1 = dGGGCGCGGGAGGAAGGGGGCGGG [60].

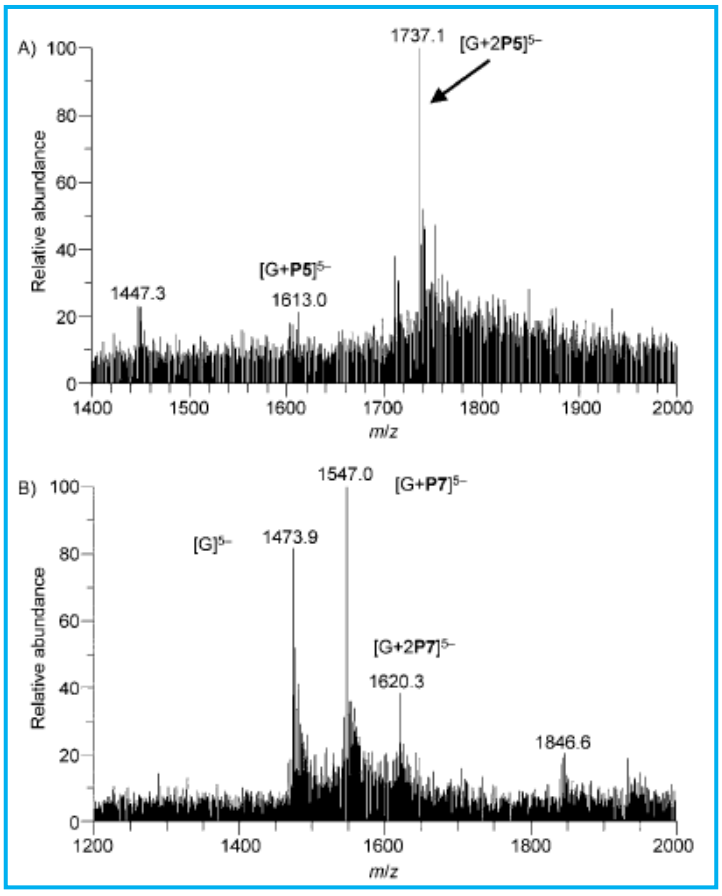

3.5. Atomic Force Microscopy

Atomic force microscopy (AFM) can be used to distinguish proteins bound to nucleic acid templates. One of the great advantages of the atomic force microscope, particularly with respect to the imaging of biological specimens, is that it can work in fluid, so that experiments can be performed under near-physiological conditions and allowing the imaging of interactions and transactions between molecules in real time [67]. AFM techniques will play a larger role in studying interactions between biological specimens, such as ligand-receptor [68] and protein-DNA [69] systems, and can also be applied to the study of drug interactions with a variety of biological specimens.

Drug-DNA complexes have been studied with AFM to determine DNA ligand mode-of-binding [70-73]. This is of considerable interest since nucleic acid ligands are commonly used as anticancer drugs and in the treatment of genetic diseases. However, determining whether they bind to DNA by intercalation within major and minor grooves, by "nonclassical" modes, or by a combination of these modes can often be difficult. AFM was used to study drug binding mode, affinity, and exclusion number by comparing the length of DNA fragments that have and have not been exposed to the drug [71]. It is known that if intercalative binding is occurring, the DNA strand increases in length. Furthermore, the degree of lengthening is informative in determining the binding affinity and the site-exclusion number. AFM was shown to be an effective means of seeing and measuring any changes in the DNA strand. e.g., when exposed to ethidium, the DNA strand was shown through AFM to have increased in length from 3300 nm to 5250 nm (Figure 16) indicating the intercalative mode of binding [70]. Similarly, AFM intercalative binding studies showed the increase in the DNA strand, from 3300 nm to 4670 nm, upon exposure to daunomycin. This technique has also successfully been applied to new drugs in which the mode of binding was unclear. e.g., exposure of 2,5-bis(4-amidinophenyl) (APF), did not produce lengthening of the DNA strands, indicating that the drug binds by nonintercalative modes [72].

AFM images of linear plasmid DNA interacted with various concentrations of vincristine sulfate and aspirin have been shown in Figure 17. The different structural changes and binding processes of the DNA occurring as a result of interactions with these two components have been successfully imaged. The binding process of vincrinstine sulfate on the linear plasmid DNA can be summarized as follows: DNA started to form loops at the low concentration of the drug, and subsequently was seen to be cut into various length DNA fragments in the higher vincristine concentrations. In the case of aspirin, the drug first bound on several initial DNA sites, and the binding region then grows larger with increasing drug concentrations. The two different DNA structural and conformational changes could be explained by the different mechanisms of the interactions with these two components: vincristine sulfate bound DNA through an intercalative action and aspirin bound through groove binding [74-76].

Figure 16: 2.5 µM scans showing (left) a ligand-free DNA strand measuring ~3300 nm; (right) an ethidium-DNA complex measuring ~5250 nm. Images courtesy of L.A. Bottomly, Georgia Institute of technology [70].

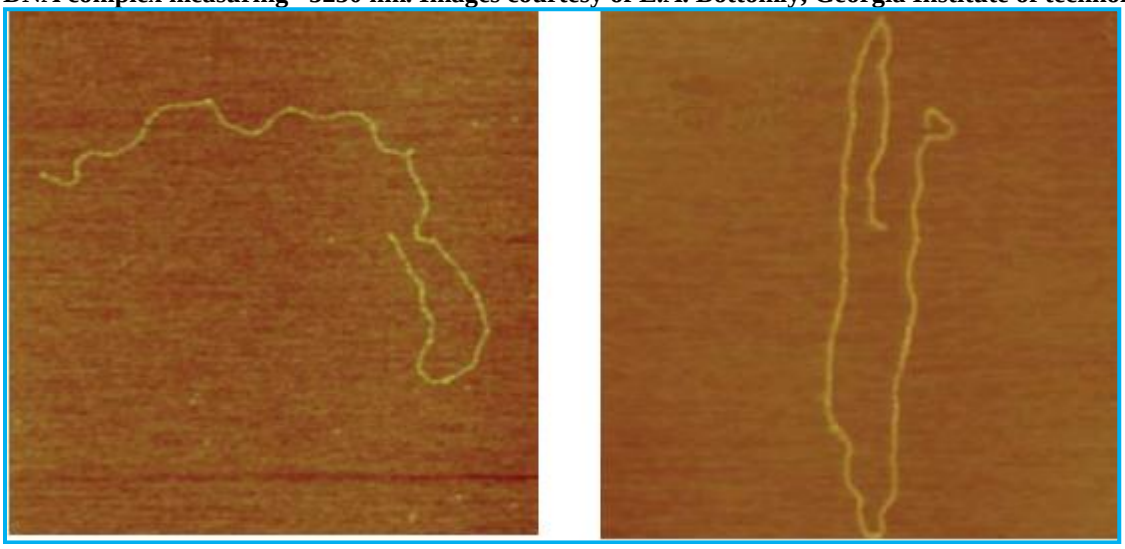

Figure 17: Naked *Eco*RV-linearized (a) form of pET28 (a+) (5.3 kbp) plasmid, the complex of 10^{-7} mol/L (b) 10^{-6} mol/l (c), 10^{-5} mol/L (d), 10^{-4} mol/L (e) aspirin and 3 ng/µL linear pET28 (a+) plasmid were imaged by AFM, using tapping mode in air. The scan size is 2.0 µm x 2.0 µm and height is coded by color in the scale from 0 nm to 5 nm [76].

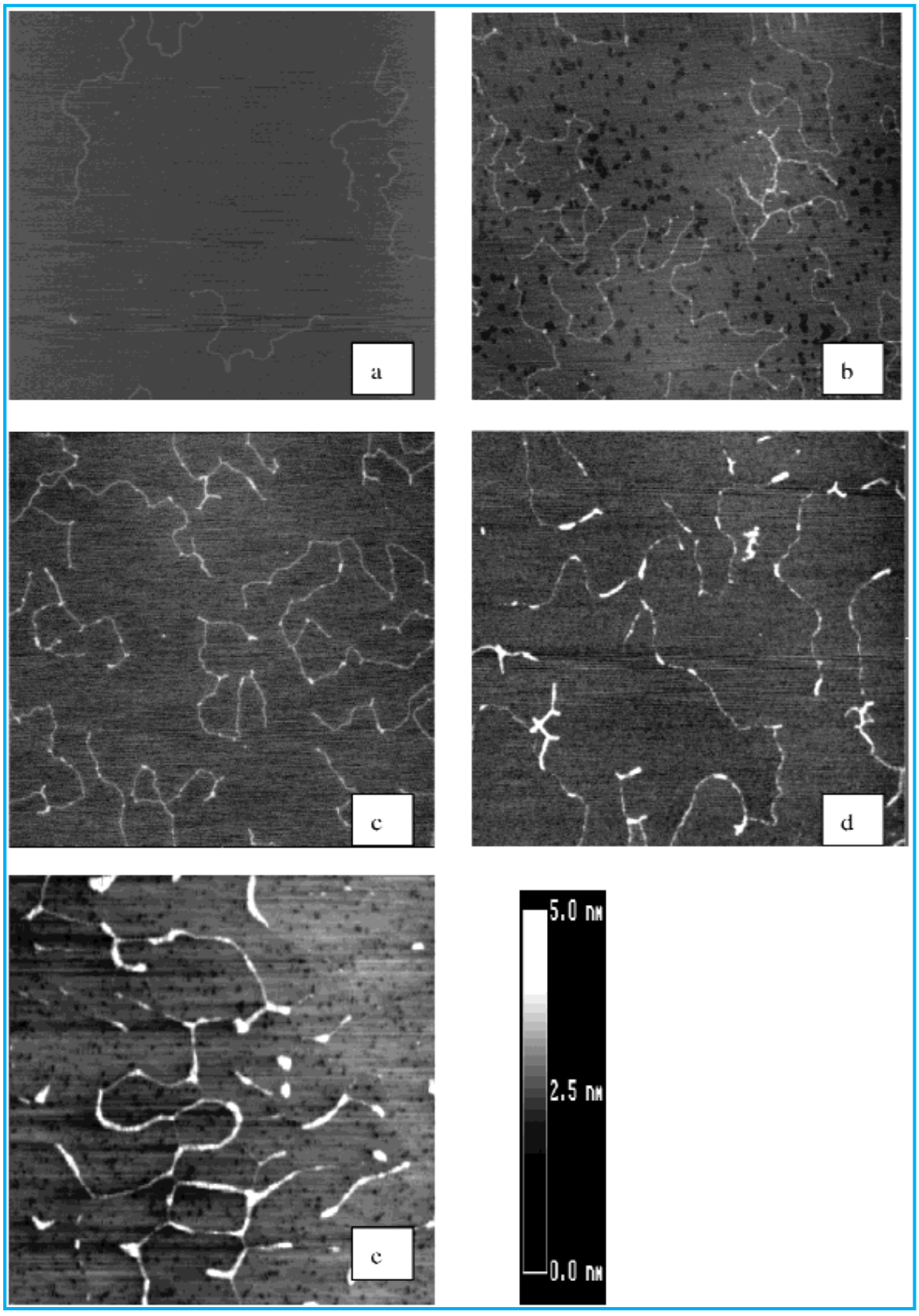

4. Conclusion

This review has focused on Drug-DNA interactions and their study by various analytical techniques like Infrared spectroscopy, Viscosity measurements, UV thermal denaturation studies, Mass spectrometry and Atomic force microsopy. These techniques are used to evaluate the binding mode as well as binding strength of the complex formed between Drug and DNA. The study should be useful for the development of potential survey for DNA structure and new therapeutic reagents for tumours and other diseases. Basically small ligand molecules (drug) interact with DNA *via* two different ways: covalent and non-covalent modes. Covalent binders act as alkylating agents as they alkylate the nucleotides of DNA. The non-covalent binders interact with *via* three different ways: intercalation, groove binding and external binding (on the outside of the helix). IR spectroscopy is a powerful tool to study interactions of DNA with drugs and the effects of such interactions in the structure of DNA, providing some insights about the mechanism of drug action. The binding stoichiometry, the relative binding affinities and the binding constants for DNA double helices of various sequences may be determined by using Mass spectrometry. AFM is used to study drug binding mode, affinity, and exclusion number by comparing the length of DNA fragments that have and have not been exposed to the drug. In case of intercalative mode the DNA strand increases in length. Furthermore, the degree of lengthening is informative in determining the binding affinity and the site-exclusion number.

Acknowledgment

The authors acknowledged the HEC Islamabad, Pakistan for financial support.

References

[1] A. Paul, S. Bhattacharya, Current Science, 102 (2) (2012) 212-231.
[2] M. Sirajuddin, S. Ali, A. Badshah, J. photochem. & photobiology B: Biology, 124 (2013) 1-19.
[3] O. Kennard, Pure & Appl. Chem. 65 (6) (1993) 1213-1222.
[4] R. Hajian, N. Shams, M. Mohagheghian, J. Braz. Chem. Soc. 20 (8) (2009) 1399-1405.
[5] M. Sechi, M. Derudas, R. Dallocchio, A. Dessì, A. Cosseddu, G. Paglietti, Letters in Drug Design & Discovery, 6 (2009) 56-62.
[6] H.K. Liu, P.J. Sadler, Acc. Chem. Res., 44 (2011) 349-359.
[7] C. Silvestri, J.S. Brodbelt, Mass Spectrom Rev., (2012) 1-20.
[8] Y. Ni, D. Lin, S. Kokot, Anal. Biochem. 352 (2006) 231-242.
[9] J.M. Kelly, A.B. Tossi, D.J. McConnell, C. Oh Uigin, Nucl. Acids Res. 13 (1985) 6017-6034.
[10] E. Froehlich, A. Gupta, J. Provencher-Mandeville, E. Asselin, J. Bariyanga, G. Berube, H.A. Tajmir-Riahi, DNA Cell Biol. 28 (1) (2009) 31-39.
[11] R. Marty, A.A. Ouameur, J.F. Neault, S. Nafisi, H.A. Tajmir-Riahi, DNA Cell Biol. 23 (3) (2004) 135-140.
[12] S. Nafisi, A. Sobhanmanesh, K. Alimoghaddam, A. Ghavamzadeh, H.A. Tajmir-Riahi, DNA Cell Biol. 24 (10) (2005) 634-640.
[13] C.N. Nsoukpoe-Kossi, C. Descoteaux, E. Asselin, J. Bariyanga, H.A. Tajmir-Riahi, G. Berube, DNA Cell Biol. 27 (6) (2008) 337-343.
[14] S.A. Lee, B. Sclavi, J.W. Powell, W. Williamson III, A. Rupprechat, Phys. Rev. E, 48 (1993) 2240-2245.
[15] Y.Z. Chen, A. Szabo, D.F. Schroter, J.W. Powell, S.A. Lee, E.W. Prohofsky, Phys. Rev. E, 55 (1997) 7414-7423.
[16] J.H. Riazance-Lawrence, H. Kang, P.J. Chou, W.C. Johnson Jr., M. Vorlickova, Biopolymers, 34 (11) (1994) 1469-1476.
[17] S. Charak, D.K. Jangir, G. Tyagi, R. Mehrotra, J. Mol. Struct. 1000 (2011) 150–154.
[18] S. Adam, J. Liquier, J.A. Taboury, E. Taillandier, Biochemistry, 25 (11) (1986) 3220-3225.
[19] J. Liquier, E. Taillandier, Infrared spectroscopy of nucleic acids, in: H.H. Mantsch, D. Chapman (Eds.), Infrared Spectroscopy of Biomolecules, Wiley-Liss, Inc, New York, 1996, pp. 131-158.
[20] S. Lee, P. Debenedetti, J. Errington, B. Pethica, D. Moore, J. Phys. Chem. B, 108 (9) (2004) 3098-3106.
[21] F.S. Parker, Nucleic Acids and Related Compounds, In: Applications of Infrared, Raman, and Resonance Raman Spectroscopy in Biochemistry, Plenum Press, New York, 1983, pp. 349-359.
[22] A. Pevsner, M. Diem, Biopolymers, 72 (4) (2003) 282-289.
[23] E. Taillandier, J. Liquier, M. Ghomi, J. Mol. Struct. 214 (1989) 185-211.
[24] E. Taillandier, J. Liquier, Methods Enzymol. 211 (1992) 307-335.
[25] M. Banyay, M. Sarkar, A. Graslund, Biophys. Chem. 104 (2) (2003) 477-488.
[26] D.K. Jangir, G. Tyagi, R. Mehrotra, S. Kundu, J. Mol. Struct. 969 (2010) 126-129.

[27] E. Mateo-Marti, C. Briones, C.M. Pradier, J.A. Martin-Gago, Biosensors and Bioelectronics, 22 (2007) 1926-1932.
[28] D.M. Loprete, K.A. Hartman, Biochemistry, 32 (1993) 4077-4082.
[29] A. Ahmed Ouameur, H.A. Tajmir-Riahi, J. Biol. Chem. 279 (2004) 42041-42054.
[30] V.V. Andrushchenko, Z. Leonenko, H. van de Sande, H. Wieser, Biopolymers, 61 (2002) 243-260.
[31] S. Nafisi, A.A. Saboury, N. Keramat, J.F. Neault, H.A. Tajmir-Riahi, J. Mol. Struct. 827 (1-3) (2006) 35-43.
[32] S. Nafisi, F.G. Kahangi, E. Azizi, N. Zebarjad, H.A. Tajmir-Riah, J. Mol. Struct. 830 (2007) 182-187.
[33] M. Sirajuddin, S. Ali, A. Haider, N.A. Shah, A. Shah, M.R. Khan, Polyhedron, 40 (1) (2012) 19-31.
[34] M. Tariq, N. Muhammad, M. Sirajuddin, S. Ali, N.A. Shah, M.R. Khan, M.N. Tahir, J. Organomet. Chem. 723 (2013) 79-89.
[35] J.L. Garcia-Gimenez, M. Gonzalez-Alvarez, M. Liu-Gonzalez, B. Macias, J. Borras, G. Alzuet, J. Inorg. Biochem. 103 (2009) 923-934.
[36] D. Li, J. Tian, W. Gu, X. Liu, S. Yan, J. Inorg. Biochem. 104 (2010) 171-179.
[37] J.L. Garcia-Gimenez, G. Alzuet, M. Gonzalez-Alvarez, M. Liu-Gonzalez, A. Castineiras, J. Borras, J. Inorg. Biochem. 103 (2009) 243-255.
[38] M. Jiang, Y. Li, Z. Wu, Z. Liu, C. Yan, J. Inorg. Biochem. 103 (2009) 833-844.
[39] Y. Hu, X. Wang, H. Pan, L. Ding, Interaction mode between Methylene blue-Sm(III) complex and herring sperm DNA, Bull. Chem. Soc. Ethiop. 26(3) (2012) 395-405.
[40] M. Sirajuddin, N. Uddin, S. Ali, M.N. Tahir, Spectrochim. Acta Part A, 116 (2013) 111-121.
[41] I. Bhat, S. Tabassum, Spectrochim. Acta A, 72 (2009) 1026-1033.
[42] S. Budagumpi, V.K. Revankar, Tran. Met. Chem. 35 (2010) 649-658.
[43] N. Shahabadi, S. Kashanian, M. Khosravi, M. Mahdavi, Tran. Met. Chem. 35 (2010) 699-705.
[44] M. Sirajuddin, S. Ali, N.A. Shah, M.R. Khan, M.N. Tahir, Spectrochim. Acta A, 94 (2012) 134-142.
[45] N. Chitrapriya, V. Mahalingam, M. Zeller, K. Natarajan, Inorg. Chim. Acta, 363 (2010) 3685-3693.
[46] F.A. Shah, M. Sirajuddin, S. Ali, S.M. Abbas, M.N. Tahir, C. Rizzoli, Inorg. Chim. Acta, 400 (2013) 159-168.
[47] C. Tan, J. Liu, L. Chen, S. Shi, L. Ji, J. Inorg. Biochem. 102 (2008) 1644-1653.
[48] K.A. Kumar, K.L. Reddy, S. Satyanarayana, Trans. Met. Chem. 35 (2010) 713-720.
[49] J. Malina, O. Novakova, B.K. Keppler, E. Alessio, V. Brabec, J. Biol. Inorg. Chem. 6 (2001) 435-445.
[50] R. Zaludova, V. Kleinwachter, V. Brabec, Biophys. Chem. 60 (1996) 135-142.
[51] Y.J. Liu, Z.H. Liang, Z.Z. Li, C.H. Zeng, J.H. Yao, H.L. Huang, F.H. Wu, Biometals, 23 (2010) 739-752.
[52] S.A. Hofstadler, R.H. Griffey, Chem. Rev. 101 (2001) 377-390.
[53] J. Beck, M.L. Colgrave, S.F. Ralph, M.M. Sheil, Mass Spectrom. Rev. 20 (2001) 61-87.
[54] F. Rosu, V. Gabelica, C. Houssier, E. De Pauw, Nucleic Acids Res. 30 (2002) e82.
[55] L. Guittat, P. Alberti, F. Rosu, S.V. Miert, E. Thetiota, L. Pietersc, V. Gabelica, E.D. Pauw, A. Ottaviania, J.F. Rioue, J.L. Mergny, Biochimie, 85 (2003) 535-547.
[56] F. Rosu, E. De Pauw, V. Gabelica, Biochimie, 90 (2008) 1074-1087.
[57] J.L. Beck, M.L. Colgrave, S.F. Ralph, M.M. Sheil, Mass Spectrom. Rev. 20 (2001) 61-87.
[58] J.S. Brodbelt, Annu. Rev. Anal. Chem. 3 (2010) 67-87.
[59] J. Jaumot, R. Gargallo, Curr. Pharm. Design, 18(14) (2012) 1900-1916.
[60] H. Li, Y. Liu, S. Lin, G.Yuan, 15 (2009) 2445-2452.
[61] H. Li, Q. Zhang, G. Yuan, Rapid. Commun. Mass. Spectrom. 24 (2010) 393-395.
[62] Z.A.E. Waller, P.S. Shirude, R. Rodriguez, S. Balasubramanian, Chem. Commun. (2008) 1467-1469.
[63] O.Y. Fedoroff, M. Salazar, H. Han, V.V. Chemeris, S.M. Kerwin, L.H. Hurley, Biochem. 37 (1998) 12367-12374.
[64] P.B. Dervan, R.W. Burli, Curr. Opin. Chem. Biol. 3 (1999) 688-693.
[65] M.L. Kopka, C. Yoon, D. Goodsell, P. Pjura, R.E. Dickerson, Proc. Natl. Acad. Sci. USA, 82 (1985) 1376-1380.
[66] F. Rosu, V. Gabelica, C. Houssier, P. Colson, E.D. Pauw, Rapid. Commun. Mass Spectrom. 16 (2002) 1729-1736.
[67] J.M. Edwardson, R.M. Henderson, Research Focus/Reviews, 9 (2) (2004) 64-71.
[68] E. Florin, V.T. Moy, H.E. Gaub, Science, 264 (1994) 415-417.
[69] C. Wyman, E. Grotkopp, C. Bustamante, H.C.M. Nelson, The EMBO Journal, 14 (1995) 117-123.
[70] J.E. Coury, L. McFail-Isom, S. Presnell, L.D. Williams, L.A. Bottemly, J. Voc. Sci. Technol. A, 13 (1995) 1746-1751.

[71] J.E. Coury, L. McFail-Isom, L.D. Williams, L.A. Bottemly, Proc. Natl. Acod. Sci. USA, 93 (1996) 12283-12286.
[72] J.E. Coury, J.R. Anderson, L. McFail-Isom, L.D. Williams, L.A. Bottemly, J. Am. Chem. Soc. 119 (1997) 3792-3796.
[73] L.H. Pope, M.C. Davies, C.A. Laughton, C.J. Roberts, S.J.B. Tendler, P.M. Williams, J. Microscopy, 199 (2000) 68-78.
[74] J.F. Neault, M. Naoui, M. Manfait, H.A. Tajmir-Riahi, F.E.B.S. Lett. 382 (1996) 26-30.
[75] D.S. Pilch, C. Yu, D. Makhey, E.J. LaVoie, A.R. Srinivasan, W.K. Olson, R.R. Sauers, K.J. Breslauer, N.E. Geacintov, L.F. Liu, Biochem. 36 (1997) 12542-12553.
[76] Y. Zhu, H. Zeng, J. Xie, L. Ba, X. Gao, Z. Lu, Microsc. Microanal. 10 (2004) 286-290.

List of abbreviations

MB = Methylene blue
AO = Acridine orange
EB = Ethidium bromide
CT-DNA = Calf thymus DNA
HS-DNA = Herring sperm DNA
SS-DNA = Salmon sperm DNA
Tris = Tris(hydroxymethyl)aminomethane
Naproxen = Hnap = 6-methoxy-α-methyl-2-naphthalene acetic acid
Nadicl = Sodium diclofenac
H_2hhmh = 2-hydroxy-N'-(3-(hydroxyimino)butan-2-ylidene)benzohydrazide
H_2bhmh = N'-(3-(hydroxyimino)butan-2-ylidene)benzohydrazide
H_2ihmh = N'-(3-(hydroxyimino)butan-2-ylidene)isonicotinohydrazide
H_2hpeh = 2-hydroxy-N'-(1-(4-hydroxy-6-methyl-2-oxo-2H-pyran-3-yl)ethylidene)benzohydrazi-de
H_2ipeh = N'-(1-(4-hydroxy-6-methyl-2-oxo-2H-pyran-3-yl)ethylidene)isonicotinohydrazide
H_2bpeh = N'-(1-(4-hydroxy-6-methyl-2-oxo-2H-pyran-3-yl)ethylidene)benzohydrazide
dmaeoxd = N,N'-bis[2-(dimethylamino)ethyl]oxamide,
ox = oxalate
Zanamivir = 5-acetamido-4-guanidino-6-(1,2,3-trihydroxypropyl)-5,6-dihydro-4H-pyran-2-carboxylic acid